$3smd\,^1D$ to $3png\,^1F$ autoionization resonances of Mg

Wei-Jan Chen,[1,2] T. K. Fang,[1] T. N. Chang,[3] T. S. Yih,[2] Chi-Kung Ni,[1] and A. H. Kung[1]
[1]*Institute of Atomic and Molecular Sciences, Academia Sinica, P.O. Box 23-166, Taipei 106, Taiwan, Republic of China*
[2]*Physics Department, National Central University, Chung-Li 320-01, Taiwan, Republic of China*
[3]*Department of Physics and Astronomy, University of Southern California, Los Angeles, California 90089-0484*
(Received 23 February 2001; published 22 February 2002)

Intense ultranarrow resonances have been observed in the photoionization of Mg from the singly excited $3smd\,^1D$ ($m=3,4,5,6$) states to the doubly excited $3png\,^1F$ ($n=5,6,7$) autoionization states using stepwise laser excitation and time-of-flight mass spectrometry detection. The reported experimental energy resolution at an order of 10^{-7} of the photon energy represents a considerable improvement over the best photon energy resolution of about one part in 10^5 for the synchrotron radiation light sources. The ultra-narrow $3png\,^1F$ resonances acquire a significant strength for the normally weak $3smd\,^1D \rightarrow 3png\,^1F$ two-electron transition due to a strong configuration interaction with an overlapping broad $3pnd\,^1F$ autoionization series and the $3s\epsilon f\,^1F$ continuum. The measured line positions and transition widths are in close agreement with the theoretical results derived from a B-spline-based configuration-interaction calculation.

DOI: 10.1103/PhysRevA.65.032717 PACS number(s): 32.80.Dz, 32.70.Jz, 32.80.Rm, 33.40.+f

I. INTRODUCTION

The spectra of the alkaline-earth atoms immediately above the first ionization threshold are dominated by resonances resulting from the strongly energy-dependent doubly excited ionization states. The photoabsorption/photoionization spectra of these divalent systems are characterized typically by two asymmetric autoionizing series, one broad and one narrow in width, caused by the simultaneous change of electronic orbitals of the two outer electrons in a double-excitation process. Theoretically, the spectrum between the first and second ionization thresholds of Mg is one of the most often studied doubly excited resonant structures for a lighter alkaline-earth atom [1–5]. In addition to photoionization from the Mg ground state, calculations have also been extended to photoionization from the bound excited states of Mg [1,2] and Mg-like ions [5]. These calculations quantify the photoionization of these species from their bound excited states. They are a part of a concerted effort to provide precise physical interpretation of multielectron interaction in many-electron systems. One of the most interesting physical features suggested by these studies is the interference between the overlapping $3pnd\,^1F$ and $3png\,^1F$ autoionization series. Chang and his co-workers, using a B-spline-based configuration interaction (BSCI) approach [2,5,6], showed that the strong $3smd\,^1D$ to $3pnd\,^1F$ transitions are dominated by an isolated-core excitation (or shake-up) of the outer md electron following a bound-bound $3s$ to $3p$ excitation [3]. Their calculations also showed the presence of extremely narrow $3png\,^1F$ ($n=5,6,7$) resonances located on top of broad $3pnd\,^1F$ resonances. These features result primarily from the energy variation of the bound component of the final-state wave function in the vicinity of the $3png\,^1F$ resonance. The effect due to transition from the initial bound state to the continuum component of the final-state wave function is relatively small. The width of the $3png\,^1F$ resonances is expected to be similar to the He $2pnd\,^1P$ resonances as both can be estimated qualitatively from a $\Delta\ell=+1$ Coulomb interaction, i.e., interaction between $1s\epsilon p$ and $2pnd$ for He and $3s\epsilon f$ and $3png$ for Mg. The calculated width of Mg $3png\,^1F$ at an order of 5×10^{-8} Ry [2–4] is consistent with the estimated width of the He $2pnd\,^1P$ resonances at an order of 10^{-8} Ry ($\sim$33 MHz) [7].

Gallagher and his co-workers observed experimentally the $3pns$ and $3pnd$ doubly excited autoionizing Rydberg series of Mg using an isolated-core excitation method with stepwise laser excitation [8,9]. Their studies provided much insight into the n dependence of Mg $3pnd$ ($J=1,3$) high Rydberg autoionization series converging to the $^2P_{1/2}$ or $^2P_{3/2}$ limit of Mg^+. The lasers used in their experiments had an energy resolution of $\sim$1.0 cm^{-1}. Consequently, they have limited their study to the broad $3pnd$ series, from $n=9$ to 40. Complementing their early works, in this paper, we report in detail a multistep multicolor laser study in Mg for transitions from the singly excited $3smd\,^1D$ ($m=3$–6) states to the ultranarrow doubly excited $3png\,^1F$ ($n=5,6,7$) autoionization states [10]. These results provide a precise quantitative comparison of experiments and theoretical calculations for the narrow $3png\,^1F$ series.

II. EXPERIMENTAL APPROACH

The experimental approach follows that initially employed by Cooke *et al.* in what they describe as an isolated-core excitation scheme [11]. One of the two valence electrons in the $3s^2\,^1S$ ground electronic state of Mg is excited to a $3smd\,^1D$ state by a two-step sequential absorption process. A single-longitudinal-mode pulsed laser (I_1) is tuned to the $3s^2\,^1S$ to $3s3p\,^1P$ resonance and excites the atom to the $3s3p\,^1P$ state. After a fixed time delay, a pulse from a second laser (I_2) transfers a portion of this population from the $3s3p\,^1P$ state to a $3smd\,^1D$ state. A third pulsed laser (I_3) then photoionizes the atom from the ^1D state. The laser I_3 is scanned to probe for autoionization resonances resulting from the $3smd\,^1D$ to $3sng\,^1F$ transitions. Figure 1 illustrates the relevant energy states of Mg and the three-excitation steps used.

 ©2002 The American Physical Society

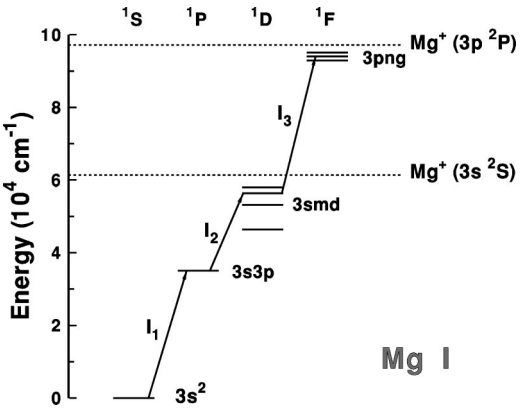

FIG. 1. Illustration of energy level scheme for the multistep three-color experiment.

The experimental apparatus is comprised of three components: a laser system, a vacuum chamber consisting of a time-of-flight (TOF) mass spectrometer connected to a Mg atomizing oven, and a data-acquisition system. The schematic diagram of the system is shown in Fig. 2.

The laser system consists of three lasers. The first laser I_1 is a CW single-frequency ring dye laser (Coherent model 699-29) that is pulse-amplified through a multistage dye amplifier pumped by a Nd:YAG laser [12]. The output energy is about 10 mJ and is 5 ns in duration. This output is frequency doubled in a KDP crystal to generate the 285.3 nm radiation needed to excite the $3s^2\,{}^1S$ to $3s3p\,{}^1P$ resonance of neutral Mg. The second laser I_2 is a grating-tuned dye laser (Lumonics model HD-300) pumped by the same Nd:YAG laser. I_2 is used to generate pulses at the wavelengths needed to excite Mg from $3s3p\,{}^1P$ to the $3smd\,{}^1D$ states. The value of these wavelengths is calculated using published data of the Mg energy levels that are accurate to 0.01 cm^{-1} [13]. The third laser I_3 is a CW Ti:sapphire single-frequency ring laser (Coherent model 899-29) that is amplified through a dye cell-Ti:sapphire crystal amplifier arrangement [14]. In order to maintain the highest resolution for the output, we removed the phase-conjugate mirror in the laser system described in Ref. [14] and used only four passes in the Ti:sapphire amplifier. The resulting pulse is about 10 ns long and has an energy of 5 mJ. This output is frequency-tripled or quadrupled by harmonic generation crystals to generate a tunable UV output of ~ 50 μJ per pulse for the experiment. The CW laser wavelength is calibrated using the laser's built-in wavemeter and an external wavemeter to an accuracy of 0.01 cm^{-1}. All three lasers are linearly polarized.

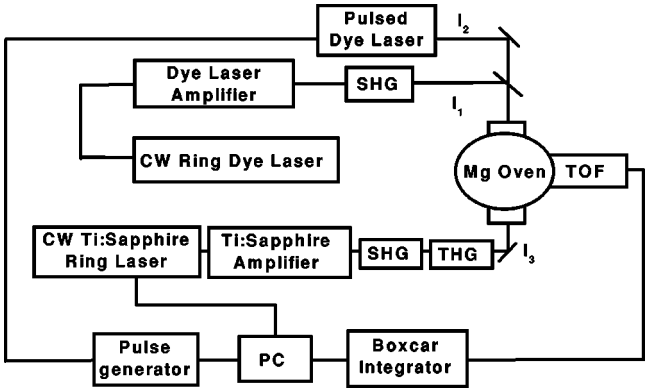

FIG. 2. Schematic diagram of the experimental setup. SHG: second-harmonic generator, THG: third-harmonic generator, TOF: time-of-flight mass spectrometer, PC: personal computer.

An effusive beam of Mg atoms is produced from a resistive oven that is isolated from the main chamber and maintained at a temperature of 450 °C. A diffusion pump in the main chamber and a turbo molecular pump in the TOF mass spectrometer maintain a background vacuum of less than 10^{-6} Torr in the vacuum system. The three lasers are each collimated to ~ 5 mm in diameter. The center portion of each beam then is passed through an iris aperture with a diameter of 1 mm. This ensures a uniform ($\pm 5\%$) intensity profile so that the excitation of the atoms in the overlapped region has a uniform spatial and concentration distribution in this multiple photon experiment. The lasers I_1 and I_2 are copropagating while I_3 is counterpropagating into the experimental chamber. The three beams overlap and cross the atomic beam at right angle at the entrance to the mass spectrometer. Ion extraction is done using two electric field plates separated by 11.5 mm. A $+150$ V extraction voltage pulse is applied to the front plate after the Mg atoms are photoionized to drive the ions through a 4-mm-diameter opening in the rear plate towards the TOF mass spectrometer. The flight path is 1 meter long. This distance is sufficient to distinguish easily the three stable isotopes of Mg. A microchannel plate detects the resulting photoions. Only the signal from the ions of the dominant isotope (^{24}Mg) is recorded.

The pulse from I_2 is delayed by 12 ns from I_1. I_3 is further delayed by 50 ns from I_2. These delays are necessary to ensure that there is no unwanted optical interference between the three laser pulses and no quantum interference between these pulses with the energy states of the atom [15]. The value of these delays is determined by experiments designed to achieve the best frequency resolution in the ionization spectrum and the least background ion interference on signal detection. Prior to the recording of each high-resolution spectrum, the intensities of I_1 and I_2 are adjusted using neutral density filters as described in the next section until I_1 and I_2 do not produce any one-color or two-color ions and there is no ion pulse broadening due to Coulomb expulsion of the ions produced by I_3. Under these conditions, the pulse energies of I_1 and I_2 are well below the detectivity of our pyroelectric energy meter of 1 μJ per pulse. I_3 is operated at the full pulse energy of 50 μJ. A delay generator is used to set the timing and to trigger the two Nd:YAG lasers at 30 Hz. The signal from the microchannel plate is amplified and fed into a boxcar integrator. Finally the data are stored in a personal computer, which is used to manage all phases of the experiment.

III. RESULTS AND DISCUSSION

The first step in the present experiment is to determine the spectral resolution. The laser I_1 excites ground state Mg to

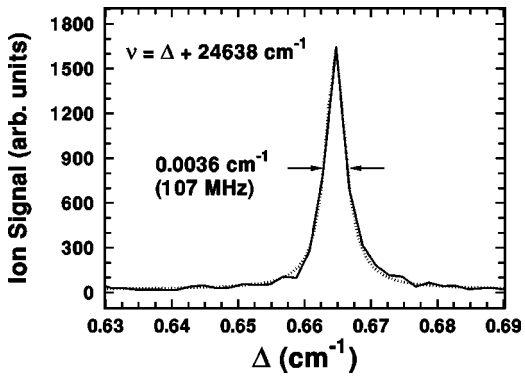

FIG. 3. High-resolution resonance-enhanced 1+1 photoionization spectrum of the $3s3p\,^1P$ state in the vicinity of the $3s8d\,^1D$ intermediate state. The solid curve is the observed data. The dotted curve is a Lorentzian fit. The laser (I_3) pulse frequency $\nu=\Delta+24\,638\ \mathrm{cm}^{-1}$.

the $3s3p\,^1P$ state. Population in the $3s3p\,^1P$ state is then ionized by resonance-enhanced $1+1$ ionization via the $3s8d\,^1D$ state by the laser I_3. The intensities of I_1 and I_3 are attenuated and the time delay between I_1 and I_3 is adjusted until the width of the intermediate resonant state in the scanned spectrum will not reduce upon further reduction of the laser intensities. The theoretical width of the $3s3p\,^1P$ to $3s8d\,^1D$ transition is given by the sum of the inverse of the lifetimes of the initial and the final energy states. The lifetime of $3s3p\,^1P$ is well-documented and is equal to 2 ns [16]. The lifetime of the $3s8d\,^1D$ state is about 94 ns [17]. For excitation using linearly polarized light, the only decay from the $3s3p\,^1P$ level in a collision-free environment is via fluorescence to the $3s^2\,^1S$ ground state. The theoretical ^1P to ^1D transition width Γ is therefore primarily determined by the ^1P to ^1S decay and can be estimated from these lifetimes to be 81 MHz. Figure 3 shows the ion signal recorded as the probe laser is scanned in wavelength. This spectral line can be fitted very well to a Lorentzian profile with a spectral full width at half maximum (FWHM) of 107 ± 2 MHz. Since the spectral profile of the Fourier-transform-limited laser is well represented by a Gaussian distribution, a deconvolution procedure detailed in the Appendix gives a spectral resolution Ω of the present experiment at 84 MHz (FWHM).

Our experimental ^1D to ^1F work was focused on the transitions from initial states of $m=3$ to 6 to final states of $n=5$ to 7. There are a total of 12 possible transitions. The transition frequency and the peak photoionization cross section of these transitions obtained from a BSCI calculation are listed in Table I. A search was performed for eight of these transitions in consideration of the laser wavelengths that were readily obtainable. In order to assist each initial search, the intensity of I_1 was increased by a factor of 10 from that established in the spectral resolution determination experiment, and I_3 was scanned for a few hundred wavenumbers to the right and to the left of the theoretically predicted spectral position of the transition. From theory, it is seen that the absorption cross section of the $3smd\,^1D$ to $3png\,^1F$ transition is 10–100 times stronger than the corresponding $3smd\,^1D$ to $3pnd\,^1F$ transitions. It is thus expected that the

TABLE I. Calculated transition energy E (cm^{-1}) and photoionization cross sections σ (10^3 Mb) for the $3smd\,^1D$ ($m=3,4,5,6$) states to the $3png\ ^1F$ ($n=5,6,7$) autoionization states of Mg.

Initial state	Final state $n=5$		$n=6$		$n=7$	
m	E	σ	E	σ	E	σ
3	46660.1	1.55	47983.7	0.79	48783.4	0.54
4	39928.5	8.85	41252.1	1.63	42051.9	0.62
5	36754.8	0.50	38078.4	2.22	38878.1	1.20
6	35039.9	5.78	36363.5	1.34	37163.3	1.11

scans would yield a weak but broad baseline feature resulting from ion signal produced due to transition to the broad $3pnd$ state and background ions, and a sharp narrow peak that corresponds to transition to the $3png\,^1F$ state. This is the criterion used to identify the existence of the $3png$ state. Indeed, in every successful spectrum, only one clearly identifiable intense but narrow peak appeared for the entire width of the scan. When a peak was observed, the intensity of I_1 was reduced to the predetermined levels, and a power dependence on I_3 of the peak strength and the peak width was measured to ensure that the signal was linear to I_3 and that the width was constant of I_3. Typically, the highest number of ions detected at the peak wavelength was about 50 per pulse. Altogether, a total of five resonances were observed. Figure 4 is a representative of the observed spectrum near the region of the sharp resonance. The resonance shown is that of the $3s4d\,^1D$ to $3p5g\,^1F$ transition. From the spectrum, the position of the peak of the $3p5g\,^1F$ state can be determined precisely using the wavelength of the laser and the known position of the lower state of the transition. The width of the transition is determined by fitting the measured resonance line to a Lorentzian profile. The assumption of a

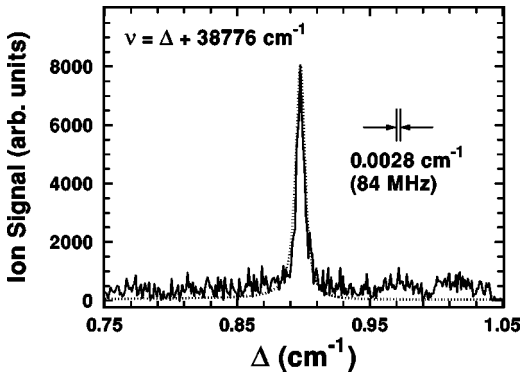

FIG. 4. Spectra of the $3s4d\,^1D$ to $3p5g\,^1F$ autoionization transition. The solid curve is recorded ion signal from the frequency scan of laser I_3. The dotted curve is a theoretical BSCI calculation of the autoionization cross section that has been convoluted with the experiment's spectral resolution. The two curves are displayed by matching the peak height and the position of the resonance. The laser (I_3) pulse frequency $\nu=\Delta+39\,776\ \mathrm{cm}^{-1}$. The experimental spectral resolution Ω of 84 MHz (i.e., 0.0028 cm^{-1}) is indicated by the two vertical bars shown.

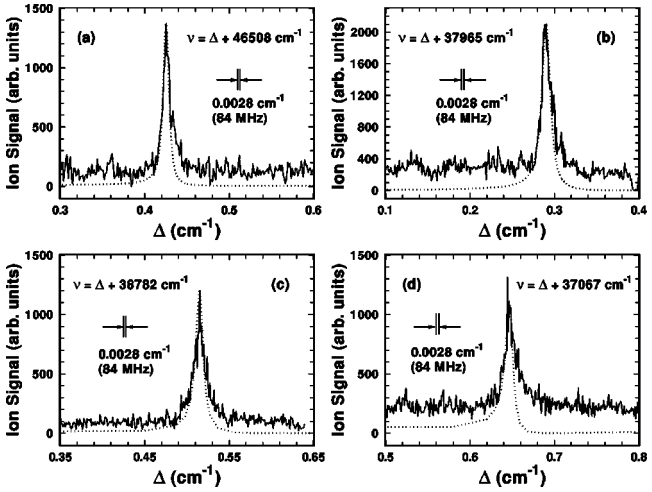

FIG. 5. Spectra of the (a) $3s3d\ ^1D$ to $3p5g\ ^1F$, (b) $3s5d\ ^1D$ to $3p6g\ ^1F$, (c) $3s5d\ ^1D$ to $3p7g\ ^1F$, and (d) $3s6d\ ^1D$ to $3p7g\ ^1F$ autoionization transitions. The solid curves are recorded ion signals from the laser scan. The dotted curves are theoretical BSCI calculation of the autoionization cross section. The dotted curves in (a) and (b) have been convoluted with the experiment's spectral resolution. In each figure, the theoretical and the experimental curves are displayed by matching the height and the position of the respective resonance peak. The laser (I_3) pulse frequency ν is expressed in terms of Δ and the experimental spectral resolution Ω of 84 MHz (i.e., 0.0028 cm^{-1}) is indicated by the two vertical bars shown.

Lorentzian line shape in place of a Fano line shape is justifiable since the observed spectral line shows a high degree of symmetry. Also displayed in Fig. 4 is the result of a BSCI calculation of the ionization cross section from $3s4d\ ^1D$ to the same region of the spectrum. For comparison purposes, the calculated peak of the ionization cross section is matched to the position and the height of the ion signal peak. The figure shows that the measured line profile and the linewidth are in very good agreement with the calculated results.

The spectra of the four other observed transitions are shown in Fig. 5. The measured transition frequencies and the experimental widths and the corresponding quantities obtained from the various calculations are shown in Table II. As is shown in the table, the measured line positions are generally in close agreement with the calculated values. However, the experimental values are uniformly to the red of the calculated values. The absolute difference is small, of the order of 100 cm^{-1} to 150 cm^{-1}, and is only about 0.2% of the total energy of the observed state. This difference in value is within the expected accuracy of the BSCI calculation that results from the use of a model potential. More work will need to be performed to determine if the persistent difference to the red is incidental or systematic. Since the low-n states included in our study are well described by LS coupling as pointed out by Gallagher [8], the quantum defect is fairly small and the effective principal quantum number n^* of these low-n states is close to integer as expected (see, e.g., Table I of Ref. [2]).

The experimental linewidths Γ, derived from Eq. (A5) of the Appendix with a measured width Γ_c at an energy resolution Ω determined earlier, are also listed in Table II. For the

TABLE II. Comparison of measured and calculated position relative to the ground state of Mg and linewidth of the *final* state of the $3smd\ ^1D$ to $3png\ ^1F$ transitions.

Transition	Final-state position (cm^{-1})	Linewidth Γ (MHz)
$3s3d\,^1D$–$3p5g\,^1F$	93063.22 [a]	249
	93053.26 [b]	1296
	93074.66 [c]	211
	92911.57(3) [d]	281(30)
$3s4d\,^1D$–$3p5g\,^1F$	93063.22 [a]	249
	93053.26 [b]	1296
	93074.66 [c]	211
	92911.60(3) [d]	169(18)
$3s5d\,^1D$–$3p6g\,^1F$	94386.78 [a]	318
	94392.03 [b]	297.4
	94398.06 [c]	358
	94273.72(3) [d]	344(35)
$3s5d\,^1D$–$3p7g\,^1F$	95186.56 [a]	308
	95090.95(3) [d]	473(50)
$3s6d\,^1D$–$3p7g\,^1F$	95186.56 [a]	308
	95090.92(3) [d]	472(50)

[a]BSCI calculation, Ref. [2].
[b]L2-based CI calculation, Ref. [3].
[c]B-spline-based stabilization method, Ref. [4].
[d]Present experiment, numbers inside the brackets are uncertainties of the most significant digit(s). The uncertainty in line position is culmulative uncertainty of the position of the intermediate state and of the wavelength of laser I_3. Uncertainty of the linewidth, resulting from the fitting of the noisy ion signal amplitude and the background, is estimated at 10% of the fitted width.

$3p5g\ ^1F$ and $3p6g\ ^1F$ states, they are $(281+169)/2=225 \pm 50$ MHz and 344 ± 35 MHz, respectively, in substantial agreement with the BSCI results, i.e., 249 MHz and 318 MHz, respectively. For the $3p7g\ ^1F$ level, the experimental value is larger by about 30% than the calculated value, still in acceptable agreement with theory. Although great care was exercised during the experiments to eliminate the effect of various broadening mechanisms such as collisions, saturation, and Coulomb expulsion, it is not surprising that small contributions from these mechanisms remain, giving a larger experimental value than the actual value. From these linewidths, a total lifetime of about 0.5 ns is obtained for the $3png\ ^1F$ states. This is quite long for energy states situated 4 eV above the ionization threshold. The radiative lifetime of the $3png\ ^1F$ to the $3sng\ ^1G$ transitions is expected to be similar to the $3s3p\ ^1P$ to $3s^2\ ^1S$ decay (i.e., about 2 ns). Hence, radiative damping [18], if it is included in the present theoretical estimate, could reduce the calculated ionization cross section significantly. The fluorescence decay from the narrow $3png\ ^1F$ resonances could possibly be observed. However, experimentally, it is a lot easier to observe the equivalent radiative fluorescence from the He $2pnd\ ^1P$ resonances, since the He $2pnd\ ^1P$ to $1snd\ ^1D$ radiative decay (i.e., the strong 21.2 eV He resonance line) is expected to occur with a lifetime between 0.5 and 0.6 ns [19].

It is clear in comparing the theoretical curves with the measured curves in Figs. 4 and 5 that there is a large off-resonance contribution in the measured signal not predicted by theory, which includes only the far wings of a single $3snd \rightarrow 3pnd$ transition. In the experiment, the observed ion signal is the total number of ions produced by the probe laser. In addition to producing ions from the $3snd$ state, the photon energy of the probe laser I_3 is sufficient to ionize the Mg atom from every other excited state. Because of the time delay imposed by the experimental conditions, several states are populated due to radiative decay from the initial $3snd\,^1D$ state. For example, the states $3s3p\,^1P$, $3s4p\,^1P$, and $3s4s\,^1S$ are energetically below the initial $3s4d\,^1D$ state and are likely to be populated before I_3 arrives. Ionization from these states and from any residual population in the $3s3p\,^1P$ state not excited by I_2 is to the featureless continuum and is likely the major contributor to the larger than predicted observed baseline ion signal. We note that in the most adverse case the strength of this baseline signal is as big as 10% of the on-resonance ion signal. This residual ion signal has made it difficult to obtain a better analysis of the line shape of these transitions.

The close agreement between experimental and theoretical results in this study supports the physical interpretation of the autoionization of the doubly excited $3pnd\,^1F$ and $3png\,^1F$ states manifested by the BSCI calculation. Photoionization from the $3snd\,^1D$ states is dominated by the shake-up of the outer d electron following the $3s$-$3p$ excitation. This shake-up process contributes substantially to the oscillator strengths for transitions from $3snd\,^1D$ states to a $3pnd\,^1F$ broad resonance and a $3png\,^1F$ narrow resonance. The experimental results reported here, however, are not sufficient to determine when the LS coupling employed in the BSCI calculation begins to take on the jj character as n increases. Further theoretical work in conjunction with these precise measurements may provide new insight into the transition from the LS to jj character for the high angular momentum autoionization series. To summarize, the multistep multicolor laser ionization, with its ultrahigh energy resolution, offers a powerful approach to study ultranarrow resonances in the VUV region not possible even with the most advanced synchrotron radiation light sources.

ACKNOWLEDGMENTS

This work is partially supported by the National Science Council of Taiwan under Contract No. NSC 87-2113-M001-017 (A.H.K.) and Contract No. NSC 88-2112-M008-011 (T.S.Y.) and by NSF Grant No. PHY9802557 (T.N.C.).

APPENDIX

In general, an isolated spectral line $L(E)$ can be represented by a Lorentzian profile,

$$L(E)=\frac{C}{\pi}\frac{\left(\frac{1}{2}\Gamma\right)}{(E-E_o)^2+\left(\frac{1}{2}\Gamma\right)^2} \tag{A1}$$

centered at an energy E_o with a width Γ, where C is an appropriate constant. If we assume that its observed spectrum $L^c(E;\Omega)$ can also be approximated by a Lozentzian profile,

$$L^c(E;\Omega)=\frac{C}{\pi}\frac{\left(\frac{1}{2}\Gamma_c\right)}{(E-E_o)^2+\left(\frac{1}{2}\Gamma_c\right)^2} \tag{A2}$$

at the same E_o with a measured width Γ_c, then $L^c(E;\Omega)$ is a convoluted spectrum of $L(E)$ using a laser spectral function in terms of a Gaussian distribution $\mathcal{G}$, i.e.,

$$L^c(E;\Omega)=\int_{-\infty}^{+\infty} L(E')\mathcal{G}(E'-E;\Omega)dE', \tag{A3}$$

where

$$\mathcal{G}(E;\Omega)=\frac{e^{-E^2/\delta^2}}{\sqrt{\pi\delta^2}}. \tag{A4}$$

The energy resolution Ω is represented by the full width at half maximum (FWHM) of the distribution function $\mathcal{G}$ and $\delta=\Omega/(2\sqrt{\ln 2})$.

Similar to the deconvolution procedure given in [20], by projecting on both sides of Eq. (A3) to the ground-state eigenfunction of a harmonic oscillator, i.e., $\Psi_0=e^{-\rho^2/2}/\pi^{1/4}$, where $\rho=\sqrt{2\ln 2}(E-E_r)/(\frac{1}{2}\Omega)$, a straightforward integration will lead to a simple relation

$$F_c(v)e^{v^2}=\sqrt{2}F_c(u)e^{u^2}, \tag{A5}$$

where $v=\sqrt{\ln 2/2}(\Gamma/\Omega)$, $u=\sqrt{\ln 2}(\Gamma_c/\Omega)$, and $F_c(x)=1-(2/\sqrt{\pi})\int_0^x e^{-y^2}dy$ is the *complementary error function*. The energy resolution Ω can be readily obtained from Eq. (A5) when the width Γ and the measured width Γ_c are known.

[1] G.N. Bates and P.L. Altick, J. Phys. B **6**, 653 (1973); C. Froese Fischer and H.P. Saha, Can. J. Phys. **65**, 772 (1987); C. Mendoza and C.J. Zeippen, Astron. Astrophys. **179**, 346 (1987); T.N. Chang and X. Tang, Phys. Rev. A **38**, 1258 (1988); R. Moccia and P. Spizzo, *ibid.* **39**, 3855 (1989); K. Butler, C. Mendoza, and C.J. Zeippen, J. Phys. B **26**, 4409 (1993); S. Mengali and R. Moccia, *ibid.* **29**, 1613 (1996).
[2] T.K. Fang and T.N. Chang, Phys. Rev. A **61**, 052716 (2000).
[3] R. Moccia and P. Spizzo, J. Phys. B **21**, 1145 (1988).
[4] T.K. Fang and Y.K. Ho, J. Phys. B **32**, 3863 (1999).
[5] T.K. Fang, B. II Nam, Y.S. Kim, and T.N. Chang, Phys. Rev. A **55**, 433 (1997).

[6] T.N. Chang and X. Tang, Phys. Rev. A **44**, 232 (1991); T. N. Chang, in *Many-body Theory of Atomic Structure and Photoionization*, edited by T. N. Chang (World Scientific, Singapore, 1993), p. 213.
[7] T.K. Fang and T.N. Chang, Phys. Rev. A **56**, 1650 (1997), and references therein.
[8] C.J. Dai, G.W. Schinn, and T.F. Gallagher, Phys. Rev. A **42**, 223 (1990).
[9] G.W. Schinn, C.J. Dai, and T.F. Gallagher, Phys. Rev. A **43**, 2316 (1991).
[10] A.H. Kung, W.J. Chen, C.K. Ni, T.K. Fang, Y.S. Yih, and T.N. Chang, Bull. Am. Phys. Soc. **44**, 722 (1999).
[11] W.E. Cooke, T.F. Gallagher, S.A. Edelstein, and R.M. Hill, Phys. Rev. Lett. **40**, 178 (1978).
[12] E. Cromwell, T. Trickl, Y.T. Lee, and A.H. Kung, Rev. Sci. Instrum. **60**, 2888 (1989).
[13] W.C. Martin and R. Zalubas, J. Phys. Chem. Ref. Data **9**, 1 (1980); S. Bashkin and J. O. Stoner, Jr., *Atomic Energy Levels and Grotian Diagrams I* (North Holland/American Elsevier, New York, 1975), p. 388.
[14] Chi-Kung Ni and A.H. Kung, Appl. Opt. **37**, 530 (1998).
[15] C.C. Wang and J.V. James, Phys. Rev. Lett. **51**, 184 (1983).
[16] A. Lurio, Phys. Rev. A **136**, A376 (1964)
[17] T.N. Chang, Phys. Rev. **41**, 4922 (1990).
[18] F. Robicheaux, T.W. Gorczyca, M.S. Pindzolz, and N.R. Badnell, Phys. Rev. A **52**, 1319 (1995); R.H. Bell and M.J. Seaton, J. Phys. B **18**, 1589 (1985).
[19] A. Kono and S. Hattori, Phys. Rev. A **29**, 2981 (1984); J. Rubensson, L. Sathe, S. Cramm, B. Kessler, S. Stranges, R. Richter, M. Alagia, and M. Coreno, Phys. Rev. Lett. **83**, 947 (1999); M.K. Odling-Smee, E. Sokell, P. Hammond, and M.A. MacDonald, *ibid.* **84**, 2598 (2000); T.W. Gorczyca, J. Rubensson, L. Sathe, M. Strom, M. Agaker, D. Ding, S. Stranges, R. Richter, and M. Alagia, *ibid.* **85**, 1202 (2000).
[20] T.K. Fang and T.N. Chang, Phys. Rev. A **57**, 4407 (1998).